Modeling and Simulation of Underwater Acoustic Communication Systems

Rafael S. Chaves, Wallace A. Martins, and Paulo S. R. Diniz

***Abstract*— This work describes a simple model for underwater acoustic (UWA) channels, taking into account Doppler effects. The performance of orthogonal frequency-division multiplexing (OFDM) systems in UWA channels is also studied. The impact of Doppler effects on OFDM transmissions is thoroughly investigated, and a simple two-step compensation strategy is described. In order to evaluate UWA models, a versatile UWA channel simulator is developed and some simulations are performed to measure the OFDM performance for time-variant channels. Those simulations evaluate the bit-error-rate and sensitivity of OFDM systems to Doppler effects. The results are satisfactory and show that only one compensation step is necessary to maintain a reasonable system performance for relative estimation errors of Doppler scaling factor in the order of 10^{-5}, corroborating that OFDM systems are suitable in some specific scenarios.**

***Keywords*— OFDM, Underwater Acoustic Channel, Doppler Effect.**

I. Introduction

Underwater communication has been attracting much attention in recent years [1], [2], [3], [4]. For instance, it is expected that those communication systems play a critical role in the investigation of climatic changes, by monitoring seismic activities and biological changes that occur in the oceans [5], [6]. Underwater communication systems can also be used to perform remote maritime exploration [7], [8], [9]. Some of those applications rely on video broadcasting, thus demanding high throughput communication systems [10].

In the aforementioned applications, the use of electromagnetic signals is prohibitive, since the attenuation in salty water is much larger than attenuation in air, calling for signals of a different nature, like acoustic signals. Indeed, acoustic signals are low-frequency mechanical waves, which are much less attenuated when propagating in an underwater environment. On the other hand, employing these signals is a very complicated task, since the underwater acoustic (UWA) noise is intense [11], [12], [13] and UWA channels feature strong time variations [2]. Moreover, UWA communication is severely degraded by Doppler effects [3] due to the low propagation speed of the acoustic waves and the ubiquitous relative motion between transmitter and receiver. Furthermore, UWA communication systems usually achieve low data rates, hindering their use in some applications [14].

In order to increase the data rates of UWA transceivers, some authors propose the use of orthogonal frequency-division multiplexing (OFDM) [1], [15], [16], [17], [18]. This work describes a simple UWA channel model based on [4], taking into account Doppler effects. Moreover, this work studies OFDM transceivers when they are employed to transmit through UWA channels and proposes a flexible UWA simulation environment. The impact of Doppler effects on those transceivers is extensively studied through numerical experiments using the proposed simulator, including a two-step Doppler compensation originally proposed in [4]. More specifically, some numerical experiments are conducted to evaluate sensitivity of OFDM systems to Doppler effects and the resulting bit-error rate (BER) performance.

This paper is organized as follows. Section II describes the UWA channel models, addressing how Doppler effects affects the channel impulse response through the presence of a Doppler scaling factor. Section III describes OFDM transceivers when working in time-variant channels. Section IV contains the simulation results. Finally, in Section V, some concluding remarks are drawn, and possible future works are described.

II. Underwater Acoustic Channel

The UWA channel can be modeled as a linear time-variant system with impulse responses given by [4]

$$h(t,\tau) = \sum_{l\in\mathcal{L}} A_l(t)\delta(\tau - \tau_l(t)), \tag{1}$$

where $\mathcal{L} = \{1,\ 2,\ \cdots,\ L\} \subset \mathbb{N}$ is the set of indexes related to all multipaths that occur in the transmission, $A_l(t) \in \mathbb{R}_+$ is the attenuation of lth multipath, and $\tau_l(t) \in \mathbb{R}_+$ is the delay associated with the lth multipath.

For a sufficiently short time interval $T_{\text{bl}} \in \mathbb{R}_+$, one can assume that $A_l(t)$ and $\tau_l(t)$ vary slowly in time, thus supporting the following reasonable assumptions:

(i) The amplitude is constant during a time interval T_{bl}:

$$A_l(t) = A_l, \quad t \in [0,\ T_{\text{bl}}). \tag{2}$$

(ii) The delay slightly varies during a time interval T_{bl} and can be approximated by a first order polynomial:

$$\tau_l(t) = \tau_l - a_l t, \quad t \in [0,\ T_{\text{bl}}), \tag{3}$$

where $\tau_l \in \mathbb{R}_+$ is the delay without relative motion between transmitter and receiver, $-a_l \in \mathbb{R}$ is the first order derivative of $\tau_l(t)$, and a_l is the Doppler scaling factor (DSF).

Based on the aforementioned assumptions, the channel impulse responses, $h(t,\tau)$, can be rewritten as

$$h(t,\tau) = \sum_{l\in\mathcal{L}} A_l\delta(\tau - (\tau_l - a_l t)), \quad t \in [0,\ T_{\text{bl}}). \tag{4}$$

Rafael S. Chaves, Wallace A. Martins, and Paulo S. R. Diniz are with both the Department of Electronics and Computer Engineering, Poli/Federal University of Rio de Janeiro, and the Electrical Engineering Program, COPPE/Federal University of Rio de Janeiro, Rio de Janeiro, RJ 21941-972, Brazil (e-mails: {rafael.chaves, wallace.martins, diniz}@smt.ufrj.br).

Thus, the channel response $\tilde{y}(t)$ to an input $\tilde{x}(t) \in \mathbb{R}$ is

$$\begin{aligned}\tilde{y}(t) &= \int_{-\infty}^{\infty} h(t,\tau)\tilde{x}(t-\tau)\mathrm{d}\tau \\ &= \sum_{l\in\mathcal{L}} A_l \tilde{x}((1+a_l)t-\tau_l), \quad t\in[0,\ T_{\mathrm{bl}}). \end{aligned} \tag{5}$$

Assuming a uniform DSF to all multipaths, i.e., $a_l = a\ \forall l \in \mathcal{L}$, then (5) can be rewritten as

$$\begin{aligned}\tilde{y}(t) &= \sum_{l=1}^{L} A_l \tilde{x}((1+a)(t-\tau_l/(1+a))) \\ &= \int_{-\infty}^{\infty} \overline{h}(\tau)\tilde{x}((1+a)(t-\tau))\mathrm{d}\tau, \quad t\in[0,\ T_{\mathrm{bl}}), \end{aligned} \tag{6}$$

where

$$\overline{h}(\tau) = \sum_{l=1}^{L} A_l \delta(\tau - \overline{\tau}_l) \tag{7}$$

is a linear time-invariant response and $\overline{\tau}_l = \tau_l/(1+a)$ is the new delay related to the lth multipath.

Equation (6) has a very simple and interesting interpretation: transmitting a signal $\tilde{x}(t)$ through a channel with impulse responses $h(t,\tau)$ with uniform DSF for all multipaths is equivalent to transmitting a signal $\tilde{x}((1+a)t)$ through a channel with linear time-invariant impulse response $\overline{h}(\tau)$ given by (7).

III. OFDM in Underwater Acoustic Channel

A. Transmitter

Let $T \in \mathbb{R}_+$ be the period of an OFDM symbol and $\mathcal{K} = \{-K/2,\ \cdots,\ K/2-1\} \subset \mathbb{Z}$ be the set of indexes of all subcarriers, with K being the number of subcarriers [19]. The subcarriers' central frequencies are placed at $f_k = k/T, \quad k \in \mathcal{K}$, in baseband transmissions. These symbols are transmitted through a channel with time-variant impulse responses given by (4) with uniform DSF.

Let $T_{\mathrm{g}} \in \mathbb{R}_+$ be the guard period of a zero-padded (ZP) OFDM [19] symbol and $T_{\mathrm{bl}} = T + T_{\mathrm{g}}$ be the total time of transmitted blocks, including the windowing operation and the guard interval, as illustrated in Fig. 1. The choice of T_{g} is very important to guarantee the proper operation of ZP-OFDM system: $T_{\mathrm{g}} \geq T_{\mathrm{ca}}$, because this choice guarantees the removal of IBI while keeping the orthogonality among subcarries [19].

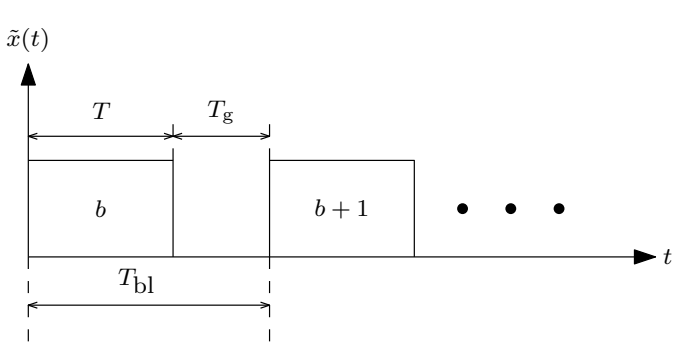

Fig. 1: Representation of b-th ZP-OFDM block.

Let $S_b[k] \in \mathcal{C} \subset \mathbb{C}$ be the symbol of a constellation $\mathcal{C}$ to be transmitted in the kth subcarrier of the bth data block. Therefore a baseband ZP-OFDM symbol is given by

$$x_b(t) = \sum_{k\in\mathcal{K}} S_b[k]\mathrm{e}^{\mathrm{j}2\pi f_k t} g(t), \quad t\in[bT_{\mathrm{bl}},\ (b+1)T_{\mathrm{bl}}], \tag{8}$$

where $g(t)$ is the pulse shaping filter [20] and $b \in \mathbb{N}$. The orthogonality of subcarriers in OFDM systems requires pulse shaping filters with a very special property, which is given by:

$$G(f) = \begin{cases} 1, & f = 0 \\ 0, & f = \frac{i}{T},\ i \in \mathbb{Z}\setminus\{0\} \\ \text{anything}, & \text{otherwise} \end{cases}, \tag{9}$$

where $G(f)$ is the Fourier transform of $g(t)$. For convenience, this work employs a rectangular pulse as pulse shaping filter. Finally, the signal to be transmitted in passband is given by

$$\tilde{x}_b(t) = 2\Re\left\{x_b(t)\mathrm{e}^{\mathrm{j}2\pi f_{\mathrm{c}} t}\right\}, \quad t\in[bT_{\mathrm{bl}},\ (b+1)T_{\mathrm{bl}}], \tag{10}$$

where $f_{\mathrm{c}} \in \mathbb{R}_+$ is the carrier frequency.

B. Receiver

In a ZP-OFDM transmission through linear time-varying channel with uniform DSF, the received passband signal is given by

$$\tilde{y}_b(t) = \sum_{l\in\mathcal{L}} A_l \tilde{x}_b((1+a)t-\tau_l) + \tilde{v}_b(t). \tag{11}$$

At the receiver, the Doppler effect must be compensated in order to enable the message recovery. This compensation is performed using a two-step compensation [4], which is divided in coarse compensation and fine compensation.

1) Coarse Compensation: At the receiver, the first processing step is the coarse compensation of the DSF [4]. Assuming that $\hat{a}$ is a good estimate of DSF, the coarse compensation is performed as a scaling in the argument of signal $\tilde{y}_b(t)$ by a factor $1/(1+\hat{a})$, yielding

$$\tilde{y}_{\mathrm{r}_b}(t) = \sum_{l\in\mathcal{L}} A_l \tilde{x}_b\left(\frac{1+a}{1+\hat{a}}t - \tau_l\right) + \tilde{v}_b\left(\frac{1}{1+\hat{a}}t\right). \tag{12}$$

The second processing step is the baseband conversion of the received signal. The received signal in baseband is given by (13) at the top of next page, where $\nu_b(t) \in \mathbb{C}$ is the baseband noise, $\varepsilon = \alpha f_{\mathrm{c}}$ and $\alpha = (a-\hat{a})/(1+\hat{a})$.

In (13) it is possible to see that the coarse compensation of DSF produces an undesired residual frequency ε. This residual frequency vanishes only if $\hat{a} = a$; however, it is extremely difficult to achieve a perfect estimation of DSF in practical situations. To verify the effect of ε in subcarriers, it is necessary to calculate the Fourier transform of the coarse compensated signal, which is given by (14) at the top of next page, where $\overline{A}_l = A_l/(1+\alpha)$, $\overline{\tau}_l = \tau_l/(1+\alpha)$, and $V_b(f) \in \mathbb{C}$ is the Fourier transform of the baseband noise.

In (14) it is possible to verify that the residual frequency ε destroys the orthogonality among subcarriers [4]. In order to recover the orthogonality it is necessary to perform a fine compensation.

$$y_{\mathrm{r}_b}(t) = \mathrm{e}^{\mathrm{j}2\pi\varepsilon t} \sum_{k\in\mathcal{K}} S_b[k] \mathrm{e}^{\mathrm{j}2\pi(1+\alpha)f_k t} \sum_{l\in\mathcal{L}} A_l \mathrm{e}^{-\mathrm{j}2\pi(f_\mathrm{c}+f_k)\tau_l} g((1+\alpha)t-\tau_l) + \nu_b(t). \tag{13}$$

$$Y_{\mathrm{r}_b}(f) = \sum_{k\in\mathcal{K}} S_b[k] \sum_{l\in\mathcal{L}} \overline{A}_l \mathrm{e}^{-\mathrm{j}2\pi(f+f_\mathrm{c})\overline{\tau}_l} G\left(\frac{f-\varepsilon}{1+\alpha} - f_k\right) + V_b(f). \tag{14}$$

2) Fine Compensation: The next step is to perform the fine compensation of DSF [4]. Assuming that $\hat{\varepsilon}$ is a good estimation of the residual frequency ε, the resulting signal $z_b(t)$ after compensation is given by

$$z_b(t) = y_{\mathrm{r}_b}(t)\mathrm{e}^{-\mathrm{j}2\pi\hat{\varepsilon}t}, \tag{15}$$

and its Fourier transform is given by (18) at the bottom of this page, where $\Delta\varepsilon = \hat{\varepsilon} - \varepsilon$. By sampling $Z_b(f)$ at frequency f_m, one has

$$Z_b[m] = \sum_{k\in\mathcal{K}} \Lambda[m,k] S_b[k] + V_b[m], \quad \forall m \in \mathcal{K}, \tag{16}$$

where $Z_b[m] = Z_b(f_m)$,

$$\Lambda[m,k] = \sum_{l\in\mathcal{L}} \overline{A}_l \mathrm{e}^{-\mathrm{j}2\pi(f_m+f_\mathrm{c}+\hat{\varepsilon})\overline{\tau}_l} G\left(\frac{f_m+\Delta\varepsilon}{1+\alpha} - f_k\right), \tag{17}$$

and $V_b[m] = V_b(f_m)$. Finally, (16) can be rewritten in a matrix form given by (19) at the bottom of this page.

IV. Simulations

In order to validate the UWA channel model described in this work, a UWA channel simulator[1] was developed and an OFDM transmission through this UWA channel was performed. The signal was transmitted through UWA channels with uniform DSF and $L \in \{3,\ 7\}$ nonzeros coefficients, where those channels were generated with delays exponentially distributed with mean $\Delta_\mathrm{m} = 1$ ms. Additionally, the gains of those channels are Rayleigh distributed with variance determined by an attenuation $\Delta P = 20$ dB during a time $T_P = 24.6$ ms. Moreover, the sampling rate used for the channels simulation was $T_s = 0.25$ μs. More details can be found in [21, p. 27-28, p. 48].

The BER performance was evaluated as a function of signal-to-noise ratio (SNR). This simulation employed a signal with bandwidth $B = 10$ kHz to achieve the same rate as in [22], [23]. A total of 1000 random data blocks was transmitted with $K = 32$ symbols of a 4-QAM constellation. A convolutional encoder was used with code rate $r_c = 0.5$, constraint length 7, generator polynomial $\mathbf{g}_0 = [133]$ and $\mathbf{g}_1 = [165]$, and a random interleaver. In the receiver, a Viterbi decoder with hard decision was used. The first block was used as pilot data for channel estimation, which was performed through a minimum mean squared error estimator. A zero forcing (ZF) equalizer was employed at the receiver working in the symbol rate. The signal was modulated by a carrier with frequency $f_\mathrm{c} = 10$ kHz. The BER was evaluated using a Monte-Carlo simulation with 10000 different channels realizations. The SNR values used in the simulations were SNR $\in \{0,\ 5,\ 10,\ 15,\ 20,\ 25,\ 30\}$ dB. The SNR definition used in this work is SNR $= 10\log_{10}(P_\mathrm{s}/P_\mathrm{n})$, where $P_\mathrm{s} \in \mathbb{R}_+$ is the signal power at the transmitter, and $P_\mathrm{n} \in \mathbb{R}_+$ is the noise power.

The BER sensitivity as a function of the estimation error in DSF was simulated. Two different simulation scenarios were analyzed: the first one just performs the coarse compensation (CC) of DSF and the second one performs the coarse and fine compensation (C&FC). The DSF estimate is $\hat{a} = (1-\epsilon)a$, where $\epsilon \in \mathcal{E}$ is the relative estimation error. The residual frequency estimate $\hat{\varepsilon}$ was assumed perfect. Two different sets $\mathcal{E}$, defined as $\mathcal{E}_1 = \{0,\ 2,\ 4,\ 6,\ 8,\ 10\} \times 10^{-5}$ and $\mathcal{E}_2 = \{0,\ 2,\ 4\} \times 10^{-4}$, were considered. The sets $\mathcal{E}_1$ and $\mathcal{E}_2$ were defined so that the intercarrier interference (ICI) did not completely degrade the symbol estimation performed by the equalizers.

Figs. 2a and 3a show BER curves when the fine compensation of DSF was not applied and the estimation error $\epsilon \in \mathcal{E}_1$. In those figures, it is possible to verify that the residual frequency ε does not have any significant influence on BER. This result is in fact expected since an estimation error in this order of magnitude does not produce any significant ICI.

Figs. 2b and 3b depict BER curves when there was fine

[1]Software available in `https://github.com/rafaelschaves/uwa-channel-simulator`.

$$Z_b(f) = \sum_{k\in\mathcal{K}} S_b[k] \sum_{l\in\mathcal{L}} \overline{A}_l \mathrm{e}^{-\mathrm{j}2\pi(f+f_\mathrm{c}+\hat{\varepsilon})\overline{\tau}_l} G\left(\frac{f+\Delta\epsilon}{1+\alpha} - f_k\right) + V_b(f). \tag{18}$$

$$\underbrace{\begin{bmatrix} Z_b\left[-\frac{K}{2}\right] \\ \vdots \\ Z_b\left[\frac{K}{2}-1\right] \end{bmatrix}}_{\mathbf{z}[b]} = \underbrace{\begin{bmatrix} \Lambda\left[-\frac{K}{2},-\frac{K}{2}\right] & \cdots & \Lambda\left[-\frac{K}{2},\frac{K}{2}-1\right] \\ \vdots & \ddots & \vdots \\ \Lambda\left[\frac{K}{2}-1,-\frac{K}{2}\right] & \cdots & \Lambda\left[\frac{K}{2}-1,\frac{K}{2}-1\right] \end{bmatrix}}_{\mathbf{\Lambda}} \underbrace{\begin{bmatrix} S_b\left[-\frac{K}{2}\right] \\ \vdots \\ S_b\left[\frac{K}{2}-1\right] \end{bmatrix}}_{\mathbf{s}[b]} + \underbrace{\begin{bmatrix} V_b\left[-\frac{K}{2}\right] \\ \vdots \\ V_b\left[\frac{K}{2}-1\right] \end{bmatrix}}_{\mathbf{v}[b]}. \tag{19}$$

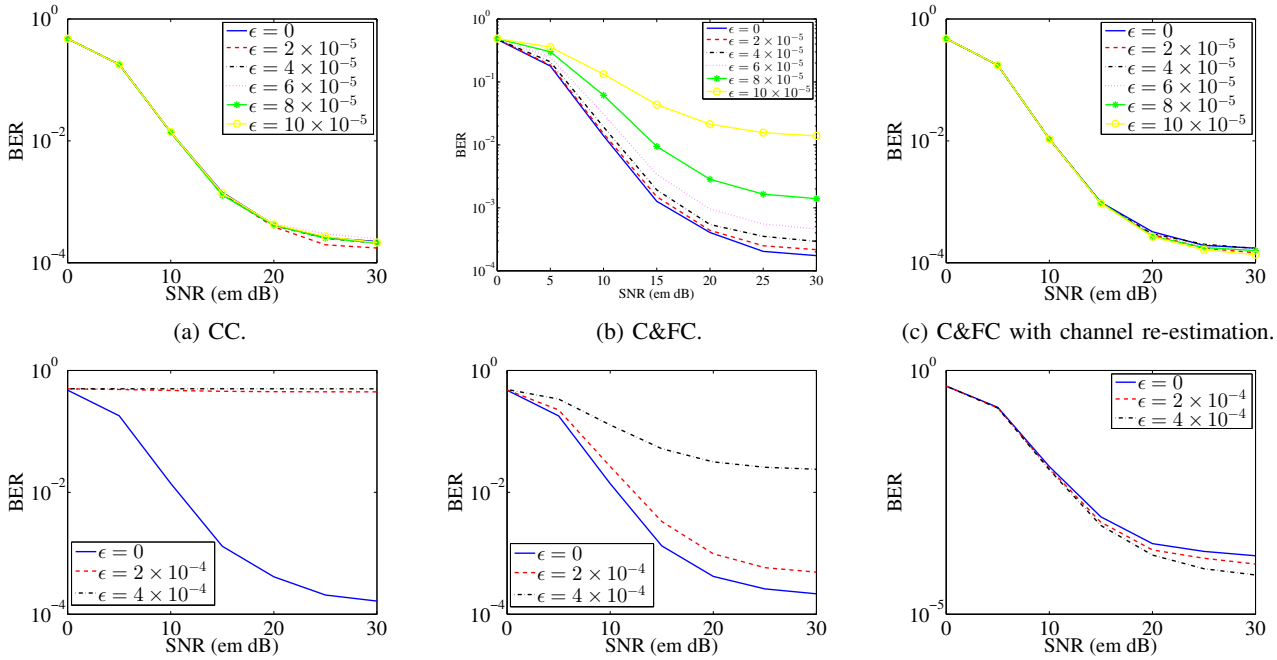

(a) CC. (b) C&FC. (c) C&FC with channel re-estimation.

(d) CC. (e) C&FC. (f) C&FC with channel re-estimation.

Fig. 2: BER *vs.* SNR using ZF equalizer for channels with $L = 3$. First row $\epsilon \in \mathcal{E}_1$ and second row $\epsilon \in \mathcal{E}_2$.

compensation of DSF and the estimation error $\epsilon \in \mathcal{E}_1$. Although the fine compensation is applied at the receiver, the BER performance is degraded as the estimation error grows. This result is expected, since the fine compensation transforms the equivalent channel in a time-varying channel, and the results presented in Figs. 2b and 3b were obtained by estimating the channel only in the first data block. As time progresses, this estimation is not accurate anymore.

Figs. 2c and 3c show the BER performance, when the channels were re-estimated at every 127 blocks for $\epsilon \in \mathcal{E}_1$. As shown in these figures, the BERs achieved when using C&FC are similar to the BERs when using CC. The results in Figs. 2c and 3c were obtained with 1000 Monte-Carlo runs.

Figs. 2d and 3d depict BER curves when the fine compensation was not performed for the residual frequency ε. Those figures show that, for an error in this order of magnitude, the residual frequency strongly impacts the system performance, unlike what happens for an error $\epsilon \in \mathcal{E}_1$.

Figs. 2e and 3e show BER curves when the fine compensation for the frequency ε was performed. In these cases, the fine compensation produces performance improvement, in comparison with the results presented in Figs. 2d and 3d. These results show that when the estimation error ϵ has a magnitude in the order of 10^{-4}, the fine compensation is necessary for the system to operate efficiently. This happens because the ICI cannot be neglected in this case, and the fine compensation attenuates its effect on the transmission.

Figs. 2f and 3f show the BER performance when the channels were re-estimated every 127 blocks and $\epsilon \in \mathcal{E}_2$. In this case, the system performance has improved when compared with the results presented in Figs. 2e and 3e.[2]

It is worth mentioning the unforeseen performance related to the different values of error ϵ. The results presented show that the errors with a larger order of magnitude reaches better performance in high SNRs values. Although this result must be carefully studied in future works, a possible justification for this fact is that the fine compensation for larger ϵ induces greater temporal diversity, which can yield channel models whose corresponding matrix forms are better conditioned.

V. Concluding Remarks

In this work, we have shown how time-varying channels with uniform Doppler scaling factor affect OFDM transmissions. Moreover, a two-step Doppler compensation was used to mitigate the Doppler effects on the subcarriers. This two-step Doppler compensation is divided into coarse and fine compensations. A functional underwater acoustic channel simulator was developed, and in order to validate the simulation environment some numerical simulations of OFDM transmissions were performed. Simulation results showed that the system performance is very sensitive to large errors in the estimation of the Doppler scaling factor. For small error values, only the coarse compensation is necessary to maintain the system performance at an acceptable level. When the error becomes larger, the fine compensation is required to keep the system operation with reasonable performance. In addition, to improve the performance further it is necessary to re-estimate the channel from time to time, because the fine compensation produces a time varying equivalent channel. Additionally, further investigation is required to address the

[2]The error floor that appears in the high SNR regime occurs due to the presence of some channels with zeroes on the unit circle.

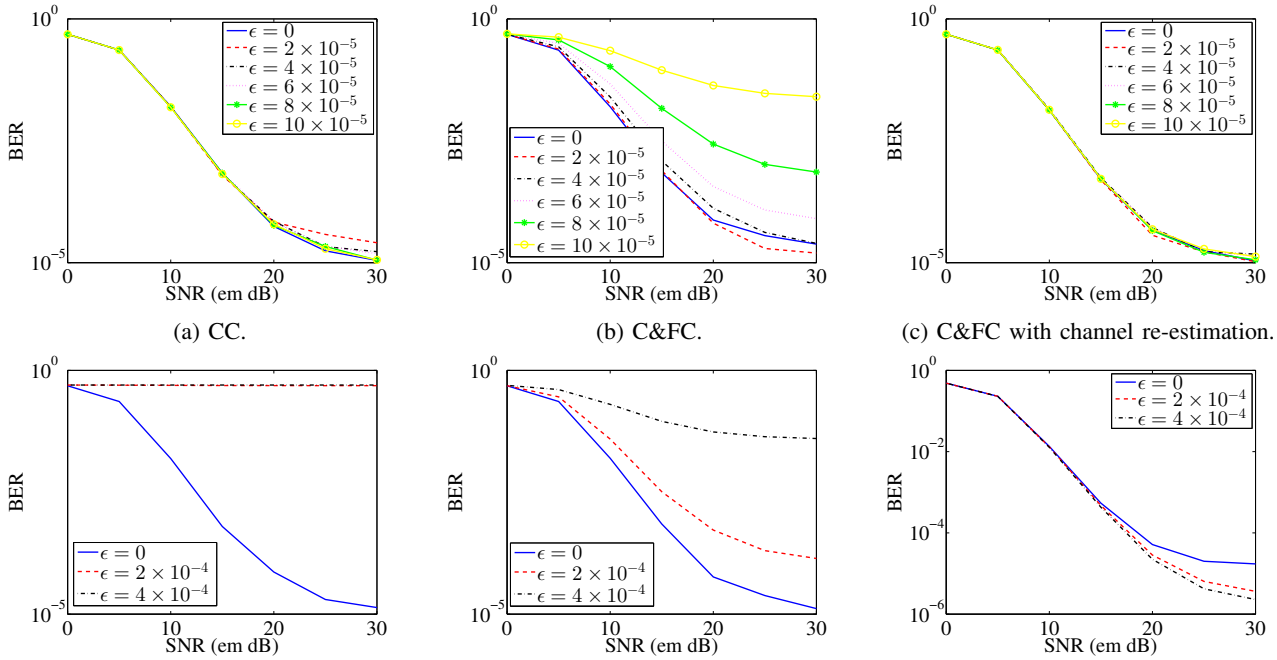

(a) CC. (b) C&FC. (c) C&FC with channel re-estimation.

(d) CC. (e) C&FC. (f) C&FC with channel re-estimation.

Fig. 3: BER *vs.* SNR using ZF equalizer for channels with $L = 7$. First row $\epsilon \in \mathcal{E}_1$ and second row $\epsilon \in \mathcal{E}_2$.

unexpected behavior of fine compensation for larger errors in the estimation of Doppler scaling factor, and evaluate the performance of OFDM systems transmitting through a time-varying channel with non-uniform Doppler scaling factor.

ACKNOWLEDGMENTS

The authors are grateful for the financial support provided by CNPq, CAPES, and FAPERJ, Brazilian research councils.

REFERENCES

[1] C. Berger, S. Zhou, J. Preisig, and P. Willett, "Sparse Channel Estimation for Multicarrier Underwater Acoustic Communication: From Subspace Methods to Compressed Sensing," *IEEE Transactions on Signal Processing*, vol. 58, no. 3, pp. 1708–1721, March 2010.

[2] C. Liu, Y. V. Zakharov, and T. Chen, "Doubly Selective Underwater Acoustic Channel Model for a Moving Transmitter/Receiver," *IEEE Transactions on Vehicular Technology*, vol. 61, no. 3, pp. 938–950, March 2012.

[3] D. Stojanovic, I. Djurovic, and S. Djukanovic, "The Effects of Doppler Scaling in Underwater Acoustic OFDM Communication," in *Mediterranean Conference on Embedded Computing*, Bar, June 2012.

[4] S. Zhou and Z. Wang, *OFDM for Underwater Acoustic Communications*. Chichester: John Wiley & Sons, May 2014.

[5] X. Du, X. Liu, and Y. Su, "Underwater Acoustic Networks Testbed for Ecological Monitoring of Qinghai Lake," in *OCEANS*. Shanghai: IEEE, April 2016, pp. 1–4.

[6] M. Arima and A. Takeuchi, "Development of an Autonomous Surface Station for Underwater Passive Acoustic Observation of Marine Mammals," in *OCEANS*. Shanghai: IEEE, April 2016, pp. 1–4.

[7] J. Heidemann, Wei Ye, J. Wills, A. Syed, and Yuan Li, "Research Challenges and Applications for Underwater Sensor Networking," in *IEEE Wireless Communications and Networking Conference*. Las Vegas: IEEE, April 2006, pp. 228–235.

[8] J.-H. Cui, J. Kong, M. Gerla, and S. Zhou, "The Challenges of Building Scalable Mobile Underwater Wireless Sensor Networks for Aquatic Applications," *IEEE Network*, vol. 20, no. 3, pp. 12–18, May 2006.

[9] J. Jin, J. Zhang, F. Shao, Z. Lv, M. Li, L. Liu, and P. Zhang, "Active and Passive Underwater Acoustic Applications Using an Unmanned Surface Vehicle," in *OCEANS*. Shanghai: IEEE, April 2016, pp. 1–6.

[10] C. Pelekanakis, M. Stojanovic, and L. Freitag, "High Rate Acoustic Link for Underwater Video Transmission," in *OCEANS*. San Diego: IEEE, September 2003, pp. 1091–1097.

[11] X. Lurton, *An Introduction to Underwater Acoustics: Principles and Applications*, 2nd ed. Chichester: Springer, 2010.

[12] J. M. Hovem, R. Vagsholm, H. Sorheim, and B. Haukebo, "Measurements and Analysis of Underwater Acoustic Noise of Fishing Vessels," in *OCEANS*. Genova: IEEE, May 2015, pp. 1–6.

[13] F. Traverso, T. Gaggero, E. Rizzuto, and A. Trucco, "Spectral Analysis of the Underwater Acoustic Noise Radiated by Ships with Controllable Pitch Propellers," in *OCEANS*. Genova: IEEE, May 2015, pp. 1–6.

[14] H.-C. Song, "How Best to Utilize Bandwidth in Underwater Acoustic Communication?" in *MTS/IEEE OCEANS*. Bergen: IEEE, June 2013, pp. 1–4.

[15] B. Li, S. Zhou, M. Stojanovic, L. Freitag, and P. Willett, "Multicarrier Communication over Underwater Acoustic Channels with Nonuniform Doppler Shifts," *IEEE Journal of Oceanic Engineering*, vol. 33, no. 2, pp. 198–209, April 2008.

[16] B. Li, J. Hueng, S. Zhou, K. Ball, M. Stojanovic, L. Freitag, and P. Willett, "MIMO-OFDM for High-Rate Underwater Acoustic Communications," *IEEE Journal of Oceanic Engineering*, vol. 34, no. 4, pp. 634–644, October 2009.

[17] M. Stojanovic, "Low Complexity OFDM Detector for Underwater Acoustic Channels," in *OCEANS*. Singapore: IEEE, September 2006, pp. 1–6.

[18] T. Kang and R. Iltis, "Iterative Carrier Frequency Offset and Channel Estimation for Underwater Acoustic OFDM Systems," *IEEE Journal on Selected Areas in Communications*, vol. 26, no. 9, pp. 1650–1661, December 2008.

[19] P. S. R. Diniz, W. A. Martins, and M. V. S. Lima, *Block Transceivers: OFDM and Beyond*. Colorado Springs: Morgan & Claypool, 2012.

[20] J. G. Proakis, *Digital Communications*, 4th ed. New York: McGraw-Hill, 2001.

[21] R. S. Chaves, "Modeling and Simulation of Underwater Acoustic Communication Systems (in Portuguese)," Graduation Thesis, Universidade Federal do Rio de Janeiro, Rio de Janeiro, 2016.

[22] Y. Shi, Z. Cao, H. Wei, S. Zhang, and W. Zhou, "DSP Implementation of OFDM-Based Underwater Acoustic Communication Transceiver," in *6th International Conference on Wireless Communications and Signal Processing*. Hefei: IEEE, October 2014, pp. 1–6.

[23] J. Younce, A. Singer, T. Riedl, B. Landry, A. Bean, and T. Arikan, "Experimental Results with HF Underwater Acoustic Modem for High Bandwidth Applications," in *49th Asilomar Conference on Signals, Systems and Computers*. Pacific Grove: IEEE, November 2015, pp. 248–252.